https://doi.org/10.5194/acp-2020-816
Preprint. Discussion started: 31 August 2020
© Author(s) 2020. CC BY 4.0 License.

Atmospheric Chemistry and Physics Discussions

Soil-atmosphere exchange flux of total gaseous mercury (TGM) in subtropical and temperate forest catchments

Jun Zhou [a, b, c], Zhangwei Wang [a, c, *], Xiaoshan Zhang [a, c], Charles T. Driscoll [d], Che-Jen Lin [e]

a. State Key Laboratory of Urban and Regional Ecology, Research Center for Eco-Environmental Sciences, Chinese Academy of Sciences, Beijing 100085, China.

b. Key Laboratory of Soil Environment and Pollution Remediation, Institute of Soil Science, Chinese Academy of Sciences, Nanjing 210008, China.

c. University of Chinese Academy of Sciences, Beijing 100049, China.

d. Department of Civil and Environmental Engineering, Syracuse University, 151 Link Hall, Syracuse, New York 13244, United States.

e. Center for Advances in Water and Air Quality, Lamar University, Beaumont, Texas 77710, United States.

* Corresponding author: Zhangwei Wang

E-mail address: wangzhw@rcees.ac.cn(Z. Wang); Phone: +86 10 62849168.

No.18 Shuangqing Road, Beijing 100085, China

First author e-mail: zhoujun@issas.ac.cn (J. Zhou); Phone: +86 25 86881319.

No.73 East Beijing Road, Nanjing 210008, China.

https://doi.org/10.5194/acp-2020-816
Preprint. Discussion started: 31 August 2020
© Author(s) 2020. CC BY 4.0 License.

Atmospheric Chemistry and Physics Discussions

Abstract: Evasion from soil is the largest source of mercury (Hg) to the atmosphere in terrestrial ecosystems. To improve understanding of controls and reduce uncertainty in estimates of forest soil-atmosphere exchange, soil-air total gaseous Hg (TGM) fluxes were measured for 130 and 96 days for each of four plots at a subtropical forest and a temperate forest, respectively. The soil-air TGM fluxes, measured using dynamic flux chambers (DFC), showed patterns of both emission and deposition at five study plots, with an area-weighted net emission rate of 3.2 and 0.32 ng m^{-2} hr^{-1} for the entire subtropical and temperate forests, respectively. At the subtropical forest, the highest fluxes and net soil Hg emission were observed for an open field, with lesser emission rates in coniferous (Masson pine) and broad-leaved (camphor) forests, and net deposition in a wetland. At the temperate forest, the highest fluxes and net soil Hg emission were observed for a wetland and an open field, with lesser emission rates in deciduous broad-leaved and deciduous needle-leaf (larch) forests, and net deposition in an evergreen pine forest (Chinese pine). High solar radiation and temperature in summer resulted in the high Hg emission at the subtropical forest, and open field and evergreen pine forest at the temperate forest. At the temperate deciduous plots, the highest Hg emission was in spring during leaf-off period due to direct solar radiation exposure to soils. Fluxes showed strong positive relationships with solar radiation and soil temperature, and negative correlations with ambient-air TGM concentration in both subtropical and temperate forests, with area-weighted compensation points of 6.82 and 3.42 ng m^{-3}, respectively. The compensation points implicated that the atmospheric TGM concentration plays a critical role in inhibiting the TGM emission from forest floor. More attention should pay to the legacy Hg stored in terrestrial surface as a more important increasing Hg emission source with the decreasing air TGM concentration recently.

Keywords: soil-air flux; dynamic flux chamber; forest type; compensation point

https://doi.org/10.5194/acp-2020-816
Preprint. Discussion started: 31 August 2020
© Author(s) 2020. CC BY 4.0 License.

Atmospheric Chemistry and Physics Discussions

1. Introduction

Mercury (Hg) is a persistent, bio-accumulative, toxic and well-known global contaminant (Obrist et al., 2018). Unlike other heavy metals in the atmosphere, the Hg mainly exists as Hg^0, which accounts more than 90% of total gaseous Hg (TGM). Due to the long longevity, atmospheric Hg^0 is able to undergo over long distances to areas without anthropogenic emissions (Kamp et al., 2018;Slemr et al., 2018). Global long-range atmospheric transport and deposition is the main pathway of Hg input to remote ecosystems (Obrist et al., 2018;Zdanowicz et al., 2018;Motta et al., 2019). Soils account for more than 90% of Hg stored in terrestrial ecosystems (Obrist, 2012), with global top soil Hg pools (0–40 cm) estimated at > 300 000 Mg (Hararuk et al., 2013;Zhou et al., 2017a). The large Hg pools not only stem from geologic sources, but also from a legacy of historically anthropogenic emission over the centuries (Obrist et al., 2014).

Many studies focus on anthropogenic Hg emissions, but Hg from natural source should be valued due to the emissions from natural reservoirs (volcanic activity and forest fires etc.) and re-emission of previous depositions of anthropogenic emissions, can be equal to or two-fold larger than anthropogenic sources (Outridge et al., 2018;Fraser et al., 2018). Recent global Hg models estimate that 3600 Mg yr^{-1} of atmospheric Hg is deposited to terrestrial surfaces, with 1000 Mg yr^{-1} re-emitted back to the atmosphere (Outridge et al., 2018). Additionally, compared to anthropogenic emissions of Hg (2500 Mg yr^{-1}), estimates of re-emissions from soil surfaces are highly uncertain (Agnan et al., 2016;Outridge et al., 2018;Wang et al., 2018). Compiling data from 132 studies, Agnan et al. (2016) found that the Earth's surface (particularly in East Asia) is an increasingly important source of total gaseous Hg (TGM) emissions, contributing up to half of the global emissions from natural sources. They estimated terrestrial TGM emissions of 607 Mg yr^{-1}, but with a large uncertainty range of −513 to 1353 Mg yr^{-1}. Additionally, a recent review also suggested that the top priorities of future study should focus on campaigns for comprehensive forest Hg behavior and more efforts in long-term Hg observation in Asia (Zhang et al., 2019).

Forest soil receives Hg input from: 1) throughfall that wash out deposited Hg (II) on foliage surface; 2) litterfall that contain foliage uptake of atmospheric Hg^0; and 3) direct dry deposition to soil from the atmosphere (Teixeira et al., 2018;Risch et al., 2017;Olson et al., 2018). Mercury outputs from forests soil occur from surface or subsurface runoff and air-surface evasion. Forest soils are highly complex media, with important characteristics that affect soil-air exchange,

https://doi.org/10.5194/acp-2020-816
Preprint. Discussion started: 31 August 2020
© Author(s) 2020. CC BY 4.0 License.

Atmospheric Chemistry and Physics Discussions

including soil physio-chemical characteristics (e.g., porosity, oxygen availability, redox potential, organic matter, and pH) (Obrist et al., 2010;Carpi et al., 2014). Other factors also influence this process, such as meteorological conditions (e.g., solar radiation, air temperature, precipitation) (Zhou et al., 2015;O'Connor et al., 2019), atmospheric chemistry (ozone, nitrate radicals) (Peleg et al., 2015;Angot et al., 2016), atmospheric TGM concentrations (Wang et al., 2007) and biological processes (Obrist et al., 2010;Chen et al., 2017). Therefore, to characterize and quantify land-atmosphere exchange of TGM, it is necessary to understand the roles of these factors in mediating this process.

Field studies have shown that elevated anthropogenic Hg emissions in South-East Asia have resulted high atmospheric Hg deposition regionally (Kumari et al., 2015;Pan et al., 2010). Forests experience highly elevated Hg loads, especially in China (Fu et al., 2015;Wang et al., 2016). The annual loading of THg to subtropical forests in China have been shown to be much higher than some forest catchments in Europe and North America (Wright et al., 2016;Larssen et al., 2008) and high Hg deposition has resulted elevated the soil Hg pools in Chinese subtropical forests (Wang et al., 2018;Wang et al., 2009). However, recent studies showed that the Hg deposition and soil Hg concentration in temperate forest were similar to those in Europe and North America (Zhou et al., 2020). Forest ecosystems not only act as Hg sinks, but can also serve as sources of previously deposited Hg. The forest area of China is 2.2×10^4 km^2, with about 50% and 40% occurring as subtropical and temperate forests, respectively. Therefore, it seems likely that subtropical and temperate forests in China, which have different climate and vegetation cover, and receives different atmospheric Hg depositions, may also show different patterns in global Hg cycles during the previous deposited Hg re-emitted back to the atmosphere.

Researches on Hg flux between forest floor and atmosphere have already been studied frequently around the world and reviewed by Zhu et al. (2016) and Agnan et al. (2016). However, the study of factors influencing Hg emission from forest soils are scarce, which causes considerable uncertainty in estimates of terrestrial sources to the atmosphere. In this paper, we present results of 130-day and 96-day, as well as multi-site (five sites in each forest) study on air-surface Hg fluxes in a temperature forest catchment of the Mt. Dongling and subtropical forest catchment of Tieshanping Forest Park (TFP) in China. The study was conducted over four seasons in both forests. The aims of this investigation were to (1) characterize the air-surface Hg fluxes in different

https://doi.org/10.5194/acp-2020-816
Preprint. Discussion started: 31 August 2020
© Author(s) 2020. CC BY 4.0 License.

Atmospheric Chemistry and Physics Discussions

terrestrial ecosystems; (2) conduct field measurements to reduce the uncertainty in air-surface fluxes of TGM in forest catchments; and (3) to estimate the Hg emission from forest soils in temperate and subtropical ozone. We hypothesize that the multi-plot and multi-seasonal study of soil-air fluxes in each forests can reduce the uncertainty of temporal patterns and spatial analysis of soil-air Hg fluxes, and improve overall understanding and estimates soil evasion from forest ecosystems.

2. Materials and methods

2.1. Study area

This study was conducted at Tieshanping Forest Park (TFP) at the subtropical zone and Xiaolongmen National Forest Park of Mt. Dongling (MDL) at the temperate zone. TFP is dominated by a Masson pine (*Pinus massoniana* Lamb.) stand (conifer) with some associated species, including camphor (*Cinnamom camphora*) and Gugertree (*Schima superba* Gardn. et Champ), which was planted in 1960s following a complete destruction of a natural Masson pine forest at Tieshanping Forest Park (TFP) (106°41.24′E, 29°37.42′N). The forest is located about 20 km northeast of Chongqing City, at an altitude from 200 to 550 m. The mean annual precipitation is 1028 mm, with 75% of the rainfall occurring from May to October. The mean annual air temperature is 18.2 °C. The total area of the study forest is 1.06×10^3 ha in the TFP (Fig. 1). The soil is typically mountain yellow earth (corresponding to an Acrisol in the FAO) (FAO, 1988), with clay mineralogy dominated by kaolinite (Zhou et al., 2018).

Mt. Dongling is near the Beijing Forest Ecosystem Research Station (BFERS), Chinese Academy of Sciences (115°26′, E40°00' N), which is located 110 km southwest of mega-city Beijing in North China. The elevation is 1300 m asl. The annual average rainfall is 612 mm and mean relative humidity is 66%. The region's climate is predominantly warm temperate continent monsoon climate with an annual average temperature 4.8 °C. Soil type is mountain brown earth (corresponding to a Eutric cambisol in FAO) (FAO, 1988). Cool and dry climate in the study area has resulted in deep litter and high organic matter concentrations (Fang et al., 2007). The study area is a mature and secondary forest protected since the 1950s following the extensive deforestation. Hg concentrations in environment media are provided in the Supporting Information (SI, Supporting Text).

https://doi.org/10.5194/acp-2020-816
Preprint. Discussion started: 31 August 2020
© Author(s) 2020. CC BY 4.0 License.

Atmospheric Chemistry and Physics Discussions

137 **2.2. Dynamic flux chamber (DFC) measurement**

138 To reduce the spatial uncertainty in Hg fluxes, different ecosystems were selected for study in
139 a sub-catchment at the subtropical TFP, including a coniferous forest (plots S-A and S-B), a wetland
140 (plot S-C), a broad-leaved (camphor) forest (plot S-D) and an open field with bare soil (plot S-E),
141 and a sub-catchment at the temperate MDL, including a Chinese pine forest (plots T-A), larch forest
142 (plots T-B), wetland (plots T-C), mixed broad-leaved forest (plots T-D) and open field (plots T-E)
143 (Fig. 1). To reduce temporal uncertainty in Hg fluxes, 130-days and 96-days of flux observations
144 were undertaken over four seasons (about one-month of continuous observations for each season,
145 except one-week for winter in MDL) (Table S1). The positions of each plot was describe in the
146 Table 1 and showed in the Fig. 1.

147 Semi-cylindrical quartz glass and open-bottom DFCs (4.71 L) were utilized during the
148 sampling campaign. The area of the DFCs over the soil surface was 20 × 30 cm, with six inlet holes
149 (1 cm diameter). At the outlet of the chamber, an orifice was connected to two exit tubes: one to a
150 regulated suction pump and the other to a gold cartridge for trapping outlet TGM. A sub-stream of
151 air was trapped by a pair of gold quartz cartridges at a flow rate of 0.5 L min^{-1}, which was measured
152 by an integrating volume flow meter. The chamber flushing flow turnover time (TOT) was 0.47 min
153 and 0.94 min for the subtropical forest and temperate forest, respectively. The Hg flux was
154 calculated using the following equation:

155 $$F = (C_0 - C_i) \times Q/A \qquad (1)$$

156 where F is the soil Hg flux (ng m^{-2} hr^{-1}); C_o and C_i are the steady state Hg concentrations (ng m^{-3})
157 of the outlet and inlet air streams, respectively, which were calculated by the Hg mass detected in
158 gold cartridges and the corresponding air volume; A is the surface area enclosed by the DFC; Q is
159 the flow rate of ambient air circulated through the DFC (10 L min^{-1} for TFP and 5 L min^{-1} for MDL).

160 High flow rates and short TOT are appropriate for measuring flux from soils with high Hg
161 concentrations or emissions, while lower flow rates and TOT are more appropriate for soils with
162 low Hg concentrations or emissions. Eckley et al. (2010) suggested that the optimal flow was at the
163 beginning of the stable $C_0 - C_i$ (ΔC) period, which was chosen as a compromise between competing
164 criteria aimed at creating conditions inside the DFC similar to the adjacent outside air. Our previous
165 study showed that when the ΔC was relative stable, the corresponding flushing flow rate was from
166 5 to 10 L min^{-1} at the subtropical forest (Zhou et al., 2017a). To void suppression the Hg emission

https://doi.org/10.5194/acp-2020-816
Preprint. Discussion started: 31 August 2020
© Author(s) 2020. CC BY 4.0 License.

Atmospheric Chemistry and Physics Discussions

potential due to the excessive buildup of Hg within the chamber, the flow rate of ambient air circulated through the DFC was 10 L min^{-1} at the subtropical forest. At the temperate forest, the soil Hg concentrations was about 3-4 times lower than those at the subtropical forest, so the lower flow rate was 5 L min^{-1} at the temperature forest.

The pair of gold cartridges were collected twice a day: every morning (about 8:00) and afternoon (about 17:00) representing night (17:00−8:00 of next day) and day (8:00−17:00) emissions, respectively. Twenty gold quartz cartridges were alternated during the sampling program. Additionally, diurnal variations of soil-air Hg fluxes were also conducted in each season, with gold cartridges collected every half an hour. A total of four diurnal measurements were conducted over the study in each forest, with diurnal variations were measured one day per season. It has been reported that the DFC method can introduce measurement bias under the given design flushing air flow rates and environmental condition (Lin et al., 2010;Zhang et al., 2002). The DFC enclosure imposes a physical constraint that can lead to accumulation to or evasion from the soil surface under measurement. Extensive examinations have been performed for selecting the experimental condition. We followed recommendations made by Eckley et al. (2010) for our measurements.

2.3. Environmental measurements

At each sampling plot, soil samples were collected from the DFC footprint (0−5 cm). Soil Hg and SOM concentrations were measured using a DMA-80 direct Hg analyzer (Milestone Ltd., Italy) and loss on ignition (LOI) method, respectively, and detailed in the SI. Soil percent moisture and temperature were monitored with Time Domain Reflectometry (TDR) Hydra Probe II (SDI−12/RS485) and a Stevens water cable tester (USA). Solar radiation was measured by a weather station (Davis Wireless Vantage VUE 06250 Weather Station, Davis Instruments, Hayward, CA) located in the TFP Forest Station and Beijing Forest Ecosystem Research Station, within about 500 m of each plot.

2.4. Quality assurance and quality control (QA/QC)

Gold cartridges were used for sampling pore TGM simultaneously with TGM flux measurements over soil. All cartridges were transported to a laboratory at the TFP Forest Station for Hg determination using a cold vapor atomic fluorescence spectroscopy (CVAFS) detector (Brooks

https://doi.org/10.5194/acp-2020-816
Preprint. Discussion started: 31 August 2020
© Author(s) 2020. CC BY 4.0 License.

Atmospheric Chemistry and Physics Discussions

Rand III). The limit of detection, based on three times the standard deviation of replicate measurements of the blank was 1 pg. Based on the sampled air volume, the detection limits were < 0.10 ng m^{-3}. The calibration curve was developed using Hg saturated air and had to have a correlation coefficient greater than 0.99 before the samples analysis could proceed. Before and after the measurement of the sampling cartridges in each day, standard Hg saturated air was injected to test the accuracy of the Hg analyzer. If the deviation of the measured Hg mass was higher than 5%, new calibration curve would be developed.

A controlled volume of saturated Hg air at a known temperature was injected to measure Hg recovery from the gold cartridges before and after the campaigns in each season. The recoveries of gold cartridges before and after the operation ranged from 98.8 to 103.2% and 96.3 to 102.5% (n=155, average=98.9%), respectively. The collection efficiency of Hg vapor by the gold cartridges was determined by connecting two cartridges in sequence and sampling the ambient air for 24 h in laboratory. For all cartridges, less than 1% Hg was detected on the second cartridges compared to the first cartridge, indicating that more than > 99% of TGM was absorbed by the gold cartridges during the field operation. For comparison, Hg fluxes were measured by two chambers side by side simultaneously. Blanks of the soil TGM flux sampling systems were measured by placing the DFC on a quartz glass surface in the five plots. The sampling time for blank measurements was same as soil-air TGM flux measurements, which were collected at 8:00 and 17:00, representing night (17:00−8:00 of next day) and day (8:00−17:00) emissions, respectively. The averaged blank was 0.13 ± 0.21 ng m^{-2} h^{-1} (n=10), which was subtracted from the soil-air TGM flux for each season.

2.5. Statistical analysis

Seasonal and annual fluxes were compared among the ten plots. Separate two-way ANOVAs were used to determine if differences in flux existed among the seasons and sites. All differences in means were significant at the p=0.05 level and all means are reported with ± one standard deviation from the mean. The correlations between environmental parameters and fluxes were analyzed by Pearson's Correlation Tests using SPSS software (SPSS Inc. 16.0) and correlation coefficient and p values are presented and significantly correlated at the level of 0.05.

3. Results and discussion

https://doi.org/10.5194/acp-2020-816
Preprint. Discussion started: 31 August 2020
© Author(s) 2020. CC BY 4.0 License.

Atmospheric Chemistry and Physics Discussions

227 **3.1. Landscape- and forest species-dependence of soil-air Hg fluxes at the forest catchment**
228 **scale**

229 The soil TGM flux measurements for the five plots were calculated for the day and night and
230 reported as mean daily fluxes with standard deviations (SD) at the subtropical forest (Fig. 2a)
231 temperate forest (Fig. 2b). Over the course of the campaigns, net TGM emission was observed at
232 the open field (24 ± 33 ng m^{-2} hr^{-1}), coniferous forest (upper elevation 2.8 ± 3.9 ng m^{-2} hr^{-1}, mid
233 elevation 3.5 ± 4.2 ng m^{-2} hr^{-1}) and the broad-leaved forest (0.18 ± 4.3 ng m^{-2} hr^{-1}), while net
234 deposition was evident at the wetland (−0.80 ± 5.1 ng m^{-2} hr^{-1}) at the subtropical forest, respectively.
235 At the temperate forest, net TGM emission was observed at the wetland (3.81 ± 0.52 ng m^{-2} hr^{-1}),
236 open field (1.82 ± 0.79 ng m^{-2} hr^{-1}), mixed broad-leaved forest (0.68 ± 1.01 ng m^{-2} hr^{-1}), larch
237 forest (0.32 ± 0.96 ng m^{-2} hr^{-1}), while net deposition was evident at the Chinese pine forest (−0.04
238 ± 0.81 ng m^{-2} h^{-1}), respectively. The fluxes at the temperature forest were 10-times lower than that
239 at the subtropical forest due to different environmental factors, such as lower temperature, solar
240 radiation and soil Hg concentrations (see section 3.3).

241 This pattern suggests that soil-air Hg fluxes at catchment scale vary by soil properties (e.g.,
242 soil Hg concentration, moisture, SOM) and forest species composition. High variability (SD and
243 coefficient of variation (SD/mean, range of 14−2374%) was evident in daily Hg fluxes largely
244 driven by meteorological variation. The fluxes at the subtropical forest plots of this study were
245 much lower than those reported for other subtropical evergreen forests in China such as Mt.
246 Gongga (0.5–9.3 ng m^{-2} hr^{-1}) (Fu et al., 2008), Mt. Jinyun (14.2 ng m^{-2} hr^{-1}) (Ma et al., 2013) and
247 Mt. Simian (11.23 ng m^{-2} hr^{-1}) (Ma et al., 2018), all of which were conducted usually in several
248 sunny days. Our flux measurements in temperate forest were slightly lower or comparable to those
249 in North American deciduous forests, ranging from −0.73 to 2.7 ng m^{-2} hr^{-1} (Choi and Holsen,
250 2009b;Hartman et al., 2009;Carpi et al., 2014;Ma et al., 2018). These results demonstrated that
251 measurements over several days may exhibit considerable temporal variability and long-term study
252 should be undertaken to reduce the uncertainty in temporal patterns.

253 The mean TGM fluxes in the open fields were about 10 and 6 times higher than that under the
254 forest canopy at the subtropical and temperate forests, respectively ($p < 0.001$). Our results are
255 consistent with Ma et al. (2013) and Xin and Gustin (2007), showing large Hg evasion following
256 forest conversion to bare soils due to direct exposure to sunlight, as fluxes were enhanced by

https://doi.org/10.5194/acp-2020-816
Preprint. Discussion started: 31 August 2020
© Author(s) 2020. CC BY 4.0 License.

Atmospheric Chemistry and Physics Discussions

increases in solar radiation and temperature. Due to frequent heavy rains at the subtropical forest catchment, a large amount of surface runoff impacted the wetland (plot S-C) and elevated runoff may have decreased Hg (96 ± 43 ng g^{-1}) and SOM in surface soils due to erosion (Table 1). This site had the lowest Hg^0 fluxes of the plots studied at the subtropical forest (overall net sink). In addition, soils in the wetland plot were mostly saturated throughout the year, limiting Hg fluxes and likely contributing to the sink behavior. In contrast, the mean annual rainfall was 40% lower at the temperate forest and the wetland was located at a relatively lower terrain. Litter from surrounding higher terrain of forest was heaped by naturally cumulative process. The cool and dry climate resulted in high organic matter and low bulk density (Fang et al., 2007), which contained high binding groups of heavy metals, leading to the highest Hg concentrations (117 ng g^{-1}) at the temperate wetland. These conditions was more conducive to biological activities, the processes of which could promote Hg^{2+} bonding in soils converting to volatile Hg^0 (Choi and Holsen, 2009b;Osterwalder et al., 2019); therefore, the wetland at the temperate forest had the highest Hg^0 fluxes of the plots studied at the temperate forest (overall net sink). Previous studies suggested that more polar water molecules were able to dissolve Hg from binding sites on the soil (Gustin, 2003;Kocman and Horvat, 2010) and high soil water often caused lower soil redox potential (Zarate-Valdez et al., 2006), both of which could facilitate Hg^{2+} converting to Hg^0. Additionally, the climate was relatively dry in north China, especially in spring, and the highest solar radiation and relatively higher temperature not only enhancing the more reduction of Hg^{2+} to Hg^0 in solid phase and liquid phase, but also increased the process of water evaporation compared to that in the other study sites. The synergistic effect on Hg flux for soil temperature and moisture can enhance water evaporation at higher temperature, which subsequently facilitates additional Hg emission from soils (Gustin and Stamenkovic, 2005;Lin et al., 2010). Therefore, the highest Hg flux was observed in the wetland, especially in spring. The main reasons for the significant difference between the two fluxes at the two wetland would be due to that the soil has been saturated with water at the subtropical forest such that Hg^0 evasion is inhibited (Gustin and Stamenkovic, 2005) (see section 3.3).

At the subtropical forest, litterfall deposition was twice as high as that in the coniferous (pine) plot (plots S-A and S-B) in the broad-leaved (camphor) plot (plot S-D) (Zhou et al., 2018), resulting in greater shielding of sunlight to the surface soil and limiting soil Hg evasion. Increases in sunlight can both increase solar radiation and soil temperature, which can enhance the photochemical

https://doi.org/10.5194/acp-2020-816
Preprint. Discussion started: 31 August 2020
© Author(s) 2020. CC BY 4.0 License.

Atmospheric Chemistry and Physics Discussions

reduction of Hg^{2+} on the soil surface and Hg^0 evasion after its formation from Hg^{2+}. In the mid-slope of the pine stand (plot S-B), soil Hg concentration was elevated compared to the upslope plot (Table 1), corresponding with higher soil Hg fluxes. At the temperate forest, the lowest Hg flux and overall deposition was observed at Chinese pine forest, which was an evergreen forest and the canopy covers in forests are expected to reduce Hg flux by limiting soil warming and solar loads. Similar at the subtropical forest, the needle biomass in the larch plot was about 2.5 times as that in the mixed broad-leaved plot (plot T-D) at the temperate forest, resulting in shielding the sunlight to the surface soil and limiting soil Hg evasion in larch plot.

The forest canopy not only influences the soil Hg concentration by atmospheric Hg deposition, but also alters soil physio-chemical properties (e.g. SOM, pH, porosity) which affect soil-air exchange. For example, the annual litterfall Hg deposition flux at the broad-leaved plot (91 μg m^{-2} yr^{-1}) was approximately two times greater than the coniferous plot (41 μg m^{-2} yr^{-1}) (Zhou et al., 2018) at the subtropical forest; conversely, the SOM and soil Hg concentration in the broad-leaved forest were lower than the coniferous forest. Moreover, litter decomposition rate was lower, but the Hg mass accumulation in the litter was much higher in the coniferous forest compared to the broad-leaved forest (Zhou et al., 2018), which resulted in seemingly inconsistent patterns between litterfall mass and SOM, as well as litterfall Hg deposition and soil Hg concentrations. At the temperate forest, the higher litterfall Hg deposition and lower litter decomposition in the larch plot compared to the broad-leaved plot (Zhou et al., 2017a), which has resulted in significant higher SOM and soil Hg concentrations (Table 1). Tree species can change soil physicochemical properties (e.g. SOM, soil Hg concentrations), which influences soil-air exchange. These biological factors may have contributed to the much lower TGM evasion in the broad-leaved plot than the coniferous plot at the subtropical forest but much higher TGM evasion in the broad-leaved plot than the coniferous (larch) plot at the temperate forest (Fig. 2).

Most studies measured soil TGM fluxes at only one location or at a single forest stand to characterize the whole ecosystem. Our observations clearly show that soil-air Hg fluxes vary substantially across different plots (Fig. 2), indicating that forest type/cover and landscape position significantly affect the TGM fluxes and therefore the flux variability among different sub-plots must be considered. Based on the areal distribution of each subtropical plot type (coniferous upland and mid-slope, broad-leaved, wetland, open) (4.6 ha) and temperate plot type (Chinese pine, larch,

https://doi.org/10.5194/acp-2020-816
Preprint. Discussion started: 31 August 2020
© Author(s) 2020. CC BY 4.0 License.

Atmospheric Chemistry and Physics Discussions

317 wetland, mixed broad-leaved and open) (5.0 ha) in the study sub-catchments (Table S1), the area-
318 weighted TGM flux was 3.2 and 0.32 ng m^{-2} hr^{-1} for the entire subtropical and temperate
319 catchments, respectively. The area-weighted TGM fluxes were 14% higher than plot S-A and 16%
320 lower than plot S-B of the Masson pine stand at the subtropical forest, and were 907% higher than
321 Chinese pine plot and 53% lower than mixed broad-leaved plot at the temperate forest, respectively.
322 The observations at several plots with diverse forest cover in this study should reduce the overall
323 uncertainty associated with soil-air fluxes of TGM in the overall forest catchment.
324
325 **3.2. Seasonal variations of soil-air Hg fluxes at the forest catchment scale**
326 Soil TGM fluxes not only exhibited clear seasonal variations at all the plots, but also were
327 responsive to seasonal and meteorological patterns. At the subtropical forest, the fluxes were
328 generally highest in the summer (Fig. 2a), which showed net emissions at all the five plots, followed
329 by spring, autumn, with the lowest values in the winter, which exhibited net deposition at all plots
330 with the exception of plot S-B. The observed seasonal variation was dependent on sunlight (Fig. 3),
331 because solar radiation drives photochemical reduction of Hg^{2+} (note the correlation between the
332 TGM fluxes and solar radiation, Fig. S1). Additionally, greater solar radiation increases temperature,
333 which promotes the production of soil Hg gas by biological and thermal processes. At the temperate
334 forest, the Hg fluxes were the highest in the deciduous forest plot (wetland, mixed broad-leaved
335 forest and larch forest) in spring before leaf-out when solar radiation could directly reach the forest
336 floor (Fig. S2). In the open field and evergreen forest (Chinese pine forest) plots, the Hg fluxes were
337 highest in summer with the highest solar radiation and temperature (Fig. 4 and Fig. S2). The lowest
338 Hg fluxes were measured in the winter at all the sites when the soil covered with snow, and overall
339 emissions were observed at open field and overall deposition was observed at the other four sites
340 (Fig. 2b).
341 We also observed strong variation in TGM evasion under different weather conditions. Rain
342 events decreased TGM fluxes at all plots in both forests (Fig. S3) as the rainwater reduced soil pore
343 space and led to reduced evasion out of the soil. Furthermore, the solar radiation and temperature in
344 rainy days was much lower than those in the sunny days at the same seasons (Fig. 3 and Fig. 4).
345 Manca et al. (2013) studied snow-air Hg exchange at Ny-Ålesund, and showed on average a little
346 net deposition -0.24 ng m^{-2} hr^{-1}, and overall deposition between -0.6 and -23.8 ng m^{-2} hr^{-1} were

https://doi.org/10.5194/acp-2020-816
Preprint. Discussion started: 31 August 2020
© Author(s) 2020. CC BY 4.0 License.

Atmospheric Chemistry and Physics Discussions

observed at agricultural areas at Northeastern China (Wang et al., 2013;Zhang et al., 2013). However, some studies showed net Hg depositions at nighttime and net emissions at daytime due to high solar radiation (Maxwell et al., 2013;Spolaor et al., 2019) and empirical models suggest that most of the Hg^0 deposited to snow was re-emitted back to the atmosphere (Durnford and Dastoor, 2011). During the campaigns in winter, the solar radiation was relatively lower, which may be the reason why net deposition occurred (Fig. 4). Additionally, refrozen ice/snow layers had elevated Hg concentrations and the deposited Hg from atmosphere could be potentially released to meltwater (Zhang et al., 2012;Perez-Rodriguez et al., 2019), which was consistent to our result that the Hg from atmospheric deposition could release to meltwater, as the snow was melting during our sampling. Therefore, the multi-seasonal observations reduce the uncertainties and bias of temporal patterns of soil-air Hg fluxes, and multi-plot observations reduce the uncertainties and bias associated with spatial analysis and improve overall ecosystem estimates soil evasion, which would confirm our hypothesis.

3.3. Correlations between environmental factors and fluxes

To investigate the correlation between soil-atmosphere fluxes and environmental factors, data from four-season study were selected, and these data offered long continuous time series for the five measurement plots in each forest (Fig. 3 and 4). According to a global database, atmospheric fluxes at Hg-enriched sites are positively correlated with substrate Hg concentrations, but this relationship is not observed at sites with lower background concentrations of soil Hg (Agnan et al., 2016). Our soil Hg fluxes were strongly correlated with soil Hg concentrations at vegetated sites (forests and wetland) at the subtropical forest (Fig. S4), but not at the temperate forest.

Photo-reduction is a major driver of TGM evasion from the Earth's surface (Howard and Edwards, 2018;Kuss et al., 2018;Gao et al., 2020), and this is due to photochemically mediated reduction that converts soil Hg^{2+} to volatile Hg^0 and enhances the Hg^0 pool in the soil pore (Xin and Gustin, 2007;Choi and Holsen, 2009a). Therefore, the elevated soil pore Hg^0 concentrations increased the potential of soil pore TGM diffusion to the atmosphere, which drives an increase of Hg emissions from soil. In all the sites, no matter the daily average fluxes (Fig. 3 and 4) and daytime fluxes (Fig. S1 and S2) were all significantly correlated with the solar radiations, and the solar radiation also raised the fluxes at daytime compare nighttime (Fig. S5). In the evergreen plots of subtropical forests (plots S-A, S-B, S-D) and temperate forest (plot T-A), the Hg fluxes were the

https://doi.org/10.5194/acp-2020-816
Preprint. Discussion started: 31 August 2020
© Author(s) 2020. CC BY 4.0 License.

Atmospheric Chemistry and Physics Discussions

most highly dependent on soil temperature compared to the solar radiation due to evergreen canopy blocking most of the solar radiation loading to the forest floor in the four seasons. The result was consistent with that under the shade of forest canopy, the flux was highly dependent on soil surface temperature and not dependent on solar radiation from the forest floor in the Adirondacks (Choi and Holsen, 2009b). The fluxes in the wetlands in both forests (plots S-C and T-C) were less strongly correlated with soil temperature compared to the other plots in both forests (Fig. S6 and S7). Generally, temperature is an important factor that promotes Hg^0 evasion after its formation from Hg^{2+} by biotic and abiotic processes in soils (Pannu et al., 2014). However, the wetland soil was largely saturated at the subtropical forest. This condition likely limited soil pore TGM release to the atmosphere, resulting in the weaker correlation between soil temperature and the fluxes. Furthermore, the Hg exchange fluxes were more dependent on solar radiation and less dependent on temperature during the leaf-off period at the temperate deciduous plots, as solar radiation was able to directly reach the ground; therefore, the Hg fluxes were more solar radiation-driven in the deciduous forests, especially in the wetland (Fig. S2 and S6).

During the campaign, significant negative correlations were evident between soil moisture and soil-air fluxes of TGM at the five plots at the subtropical forest (r^2= 0.03−0.39, $p < 0.05$ for all, Fig. S8), but there was no significant correlations at the temperate forest (Fig. S9). Generally there is an optimum soil moisture condition that maximizes soil TGM flux (Gustin and Stamenkovic, 2005;Lin et al., 2010;Obrist et al., 2014;Osterwalder et al., 2018;Johnson et al., 2003), which ranges from 60% to 80% of a soil's water holding capacity (Pannu et al., 2014). A laboratory experiment using undisturbed soil collected from the our subtropical study area showed that increasing soil moisture from 2% to 20% increased the TGM flux 80% at 24 °C (Wang et al., 2014). A second field experiment was conducted to study the effects of higher soil moisture on TGM flux at the subtropical forest, showing that increasing soil moisture gradually decreased the soil Hg emissions over the range of 31−39% (Zhou et al., 2017b). Combining the results of these experiments, the soil Hg fluxes at the subtropical forest catchment should increase from low values of soil moisture reaching an optimum in the range of 20-30% and then decreasing with increasing soil moisture above these values. In this study, we also observed if the soil moisture was relatively dry (no rainfall for long time), the precipitation enhanced the Hg fluxes in both forests; however, the following rainfall events did not enhance or decreased the Hg fluxes due to higher soil moistures and lower solar

https://doi.org/10.5194/acp-2020-816
Preprint. Discussion started: 31 August 2020
© Author(s) 2020. CC BY 4.0 License.

Atmospheric Chemistry and Physics Discussions

radiations (Fig. 3 and 4). Additionally, Lin et al. (2010) observed the synergistic effects (20–30 % of additional flux enhancement) between air temperature (15 and 30 °C) and soil moisture (2.5 and 27.5 %). Perennially humid weather results in relatively high soil moisture at the subtropical forest (largely > 25% during the campaigns). Considering the relatively high bulk density and low porosity of soil at the subtropical forest (Sørbotten, 2011), soil moisture likely exceeded the optimum range for TGM evasion during the campaigns resulting in significantly negative correlations (Fig. S8). In contrast, lower bulk density and higher soil porosity would result in higher optimum range of soil moisture at the temperate forest. Moreover, the large span of the soil moisture ranged from 2 to 60% in the five plots combined with the synergistic effects of soil moisture with temperature (Lin et al., 2010), resulted in moisture was not a main driver of TGM evasion from the temperate soils.

Soil-air Hg fluxes also showed significant negative correlations with atmospheric TGM concentrations at the ten plots at both forests ($r^2 = 0.023–0.26$, $p < 0.05$, Fig. 5 and 6). According to the two-resistance exchange interface model, the exchange fluxes are controlled by the gradient of TGM concentrations at both interfaces (Zhang et al., 2002), and therefore elevated atmospheric TGM concentrations should decrease the diffusion of soil pore TGM to the atmosphere. These results are consistent with an experiment at this subtropical forest, where artificially increasing ambient-air TGM concentrations significantly inhibited soil Hg volatilization (Zhou et al., 2017b). Xin and Gustin (2007) and Gustin et al. (2006) defined an associated compensation point concept for soils, which is the atmospheric Hg concentration at which the net Hg flux between the soil and the atmosphere was zero. If the atmospheric TGM concentration is above compensation point, atmospheric deposition occurs, if below it, soil emission occurs. A strong linear relationships are shown in Fig. 5 and 6 ($p < 0.01$), giving the compensation points as 2.47, 2.97, 6.00, 3.33 and 3.50 ng m^{-3} for Chinese pine, larch, wetland, mixed broad-leaved forests and open field at the temperate forest with area-weighted compensation point of 3.42 ng m^{-3}. The compensation points were much higher at the subtropical forest, and were 6.50, 7.71, 3.92, 3.83 and 12.91 for Masson pine upland and mid-slope, wetland, broad-leaved and open field at the subtropical forest with area-weighted compensation point of 6.82 ng m^{-3}.

Diurnal variation in soil-air TGM fluxes were measured in plot S-A at the subtropical forest (Fig. 7) and in plot T-D at the temperate forest (Fig. 8). Soil TGM fluxes were well correlated with soil and air temperature ($p < 0.01$ for all) and were highly dependent on solar radiation in spring,

https://doi.org/10.5194/acp-2020-816
Preprint. Discussion started: 31 August 2020
© Author(s) 2020. CC BY 4.0 License.

Atmospheric Chemistry and Physics Discussions

summer and autumn ($p < 0.01$ for all) but not in winter ($p > 0.05$), which are similar to patterns from other studies (Howard and Edwards, 2018;Osterwalder et al., 2018;Johnson et al., 2003). Solar radiation has been shown to promote photochemical reduction of soil-bound Hg and enrich Hg^0 in soil pore gas. This reaction is kinetically enhanced at higher temperatures (Eckley et al., 2015;Lin et al., 2010;Zhang et al., 2001). Compared to the other three seasons, the relatively low soil temperature (5.95 °C at the subtropical forest and –5.66 °C at the temperate forest) may have limited the relationship between soil TGM flux and solar radiation during the winter season.

4. Conclusions and study implications

Prior to undertaking this measurement of Hg air-surface exchange flux, no direct measurement of Hg exchange flux were available for background landscapes in North China. Our high-quality direct observations can have critical implications for the role of forests in global and regional Hg cycles. Through multi-plot measurements over 130 and 96 days at the subtropical and temperate forests in China, we were able to reduce the uncertainty of soil-atmosphere TGM fluxes at the catchment scale and improve understanding of how landscape attributes to the variability in soil Hg evasion. It is inferred that forest soils acts as net TGM sources to the atmosphere, with the area-weighted TGM fluxes of 3.2 and 0.32 ng m^{-2} hr^{-1} for the entire subtropical and temperate catchments, respectively. Strong correlations were showed between the Hg flux and the climatic variables in some plots, such as solar radiation, temperature, soil moisture and air TGM concentrations. The compensation points were from some of the first full-scale field data to clearly demonstrate compensation points for background forest soils, with the area-weighted compensation point of 6.82 and 3.42 ng m^{-3} for the entire subtropical and temperate catchments, respectively. The compensation points implicated that the atmospheric TGM concentration plays critical role in inhibiting the TGM fluxes between forest floor and atmosphere. Additionally, future studies need to focus on forest soils as an important increasing source, because recent studies showed decline in anthropogenic Hg emission and TGM concentrations (Liu et al., 2019). More TGM re-emission would be from the legacy Hg stored in terrestrial surface.

Data availability. The data will be available upon request to the corresponding author.

https://doi.org/10.5194/acp-2020-816
Preprint. Discussion started: 31 August 2020
© Author(s) 2020. CC BY 4.0 License.

Atmospheric Chemistry and Physics Discussions

Author contributions. ZW and XZ conceived the experiment; JZ conducted the measurements; JZ wrote the paper with inputs from CTD, CL and ZW. All authors reviewed the manuscript.

Competing interests. The authors declare that they have no conflict of interest.

Acknowledgements. This work was funded by the Natural Science Foundation of China (No.41371461 and No. 41673113), the National Basic Research Program of China (973 Program; 2013CB430002), and "Strategic Priority Research Program" of the Chinese Academy of Sciences (grant XDB14020205). The authors would like to thank Mingquan Zou and Beijing Forest Ecosystem Research Station, Chinese Academy of Sciences, for the help in our sampling.

References:

Agnan, Y., Le, D. T., Moore, C., Edwards, G., and Obrist, D.: New constraints on terrestrial surface-atmosphere fluxes of gaseous elemental mercury using a global database, Environmental Science & Technology, 50, 507−524, 10.1021/acs.est.5b04013, 2016.

Angot, H., Dastoor, A., De Simone, F., Gardfeldt, K., Gencarelli, C. N., Hedgecock, I. M., Langer, S., Magand, O., Mastromonaco, M. N., Nordstrom, C., Pfaffhuber, K. A., Pirrone, N., Ryjkov, A., Selin, N. E., Skov, H., Song, S., Sprovieri, F., Steffen, A., Toyota, K., Travnikov, O., Yang, X., and Dommergue, A.: Chemical cycling and deposition of atmospheric mercury in polar regions: review of recent measurements and comparison with models, Atmospheric Chemistry and Physics, 16, 10735-10763, 10.5194/acp-16-10735-2016, 2016.

Carpi, A., Fostier, A. H., Orta, O. R., dos Santos, J. C., and Gittings, M.: Gaseous mercury emissions from soil following forest loss and land use changes: Field experiments in the United States and Brazil, Atmospheric Environment, 96, 423-429, 10.1016/j.atmosenv.2014.08.004, 2014.

Chen, Y., Yin, Y., Shi, J., Liu, G., Hu, L., Liu, J., Cai, Y., and Jiang, G.: Analytical methods, formation, and dissolution of cinnabar and its impact on environmental cycle of mercury, Critical Reviews in Environmental Science and Technology, 47, 2415-2447, 10.1080/10643389.2018.1429764, 2017.

Choi, H.-D., and Holsen, T. M.: Gaseous mercury emissions from unsterilized and sterilized soils: The effect of temperature and UV radiation, Environmental Pollution, 157, 1673-1678, 10.1016/j.envpol.2008.12.014, 2009a.

Choi, H. D., and Holsen, T. M.: Gaseous mercury fluxes from the forest floor of the Adirondacks, Environmental Pollution, 157, 592, 2009b.

Durnford, D., and Dastoor, A.: The behavior of mercury in the cryosphere: A review of what we know from observations, Journal of Geophysical Research: Atmospheres, 116, 10.1029/2010jd014809, 2011.

Eckley, C. S., Gustin, M., Lin, C. J., Li, X., and Miller, M. B.: The influence of dynamic chamber design and operating parameters on calculated surface-to-air mercury fluxes, Atmospheric Environment, 44, 194-203, 10.1016/j.atmosenv.2009.10.013, 2010.

Eckley, C. S., Blanchard, P., Mclennan, D., Mintz, R., and Sekela, M.: Soil–air mercury flux near a large

https://doi.org/10.5194/acp-2020-816
Preprint. Discussion started: 31 August 2020
© Author(s) 2020. CC BY 4.0 License.

industrial emission source before and after closure (Flin Flon, Manitoba, Canada), Environmental Science & Technology, 49, 9750-9757, 2015.

Fang, J., Liu, G., Zhu, B., Wang, X., and Liu, S.: Carbon budgets of three temperate forest ecosystems in Dongling Mt., Beijing, China, Science in China Series D-Earth Sciences, 50, 92-101, 10.1007/s11430-007-2031-3, 2007.

FAO: UNESCO soil map of the world, revised legend, in, World Res. Rep., 138, 1988.

Fraser, A., Dastoor, A., and Ryjkov, A.: How important is biomass burning in Canada to mercury contamination?, Atmospheric Chemistry and Physics, 18, 7263-7286, 10.5194/acp-18-7263-2018, 2018.

Fu, X., Feng, X., and Wang, S.: Exchange fluxes of Hg between surfaces and atmosphere in the eastern flank of Mount Gongga, Sichuan province, southwestern China, Journal of Geophysical Research-Atmospheres, 113, 253-270, 2008.

Fu, X. W., Zhang, H., Yu, B., Wang, X., Lin, C. J., and Feng, X. B.: Observations of atmospheric mercury in China: a critical review, Atmospheric Chemistry and Physics, 15, 9455-9476, 10.5194/acp-15-9455-2015, 2015.

Gao, Y., Wang, Z., Zhang, X., and Wang, C.: Observation and estimation of mercury exchange fluxes from soil under different crop cultivars and planting densities in North China Plain, Environmental pollution, 259, 113833, 10.1016/j.envpol.2019.113833, 2020.

Gustin, M. S.: Are mercury emissions from geologic sources significant? A status report, Science of the Total Environment, 304, 153, 2003.

Gustin, M. S., and Stamenkovic, J.: Effect of watering and soil moisture on mercury emissions from soils, Biogeochemistry, 76, 215-232, 2005.

Gustin, M. S., Engle, M., Ericksen, J., Lyman, S., Stamenkovic, J., and Xin, M.: Mercury exchange between the atmosphere and low mercury containing substrates, Applied Geochemistry, 21, 1913-1923, 2006.

Hararuk, O., Obrist, D., and Luo, Y.: Modelling the sensitivity of soil mercury storage to climate-induced changes in soil carbon pools, Biogeosciences, 10, 2393-2407, 2013.

Hartman, J. S., Weisberg, P. J., Pillai, R., Ericksen, J. A., Kuiken, T., Lindberg, S. E., Zhang, H., Rytuba, J. J., and Gustin, M. S.: Application of a rule-based model to estimate mercury exchange for three background biomes in the continental United States, Environmental Science & Technology, 43, 4989-4994, 10.1021/es900075q, 2009.

Hou, H. Y.: Vegetation Map of P.R. China(1:4, 000, 000), Beijing, 1982.

Howard, D., and Edwards, G. C.: Mercury fluxes over an Australian alpine grassland and observation of nocturnal atmospheric mercury depletion events, Atmospheric Chemistry and Physics, 18, 129-142, 10.5194/acp-18-129-2018, 2018.

Johnson, D. W., Benesch, J. A., Gustin, M. S., Schorran, D. S., Lindberg, S. E., and Coleman, J. S.: Experimental evidence against diffusion control of Hg evasion from soils, Science of the Total Environment, 304, 175, 2003.

Kamp, J., Skov, H., Jensen, B., and Sorensen, L. L.: Fluxes of gaseous elemental mercury (GEM) in the High Arctic during atmospheric mercury depletion events (AMDEs), Atmospheric Chemistry and Physics, 18, 6923-6938, 10.5194/acp-18-6923-2018, 2018.

Kocman, D., and Horvat, M.: A laboratory based experimental study of mercury emission from contaminated soils in the River Idrijca catchment, Atmospheric Chemistry and Physics, 10, 1417-1426, 2010.

https://doi.org/10.5194/acp-2020-816
Preprint. Discussion started: 31 August 2020
© Author(s) 2020. CC BY 4.0 License.

550 Kumari, A., Kumar, B., Manzoor, S., and Kulshrestha, U.: Status of Atmospheric Mercury Research in
551 South Asia: A Review, Aerosol and Air Quality Research, 15, 1092-1109, 10.4209/aaqr.2014.05.0098,
552 2015.
553 Kuss, J., Krueger, S., Ruickoldt, J., and Wlost, K.-P.: High-resolution measurements of elemental
554 mercury in surface water for an improved quantitative understanding of the Baltic Sea as a source of
555 atmospheric mercury, Atmospheric Chemistry and Physics, 18, 4361-4376, 10.5194/acp-18-4361-
556 2018, 2018.
557 Larssen, T., de Wit, H. A., Wiker, M., and Halse, K.: Mercury budget of a small forested boreal catchment
558 in southeast Norway, Science of the Total Environment, 404, 290-296,
559 10.1016/j.scitotenv.2008.03.013, 2008.
560 Lin, C. J., Gustin, M. S., Singhasuk, P., Eckley, C., and Miller, M.: Empirical models for estimating
561 mercury flux from soils, Environmental Science & Technology, 44, 8522-8528, 2010.
562 Liu, K., Wu, Q., Wang, L., Wang, S., Liu, T., Ding, D., Tang, Y., Li, G., Tian, H., Duan, L., Wang, X., Fu,
563 X., Feng, X., and Hao, J.: Measure-specific effectiveness of air pollution control on China's
564 atmospheric mercury concentration and deposition during 2013-2017, Environmental Science &
565 Technology, 53, 8938-8946, 10.1021/acs.est.9b02428, 2019.
566 Ma, M., Wang, D., Sun, R., Shen, Y., and Huang, L.: Gaseous mercury emissions from subtropical
567 forested and open field soils in a national nature reserve, southwest China, Atmospheric Environment,
568 64, 116-123, 2013.
569 Ma, M., Sun, T., Du, H., and Wang, D.: A Two-Year Study on Mercury Fluxes from the Soil under
570 Different Vegetation Cover in a Subtropical Region, South China, Atmosphere, 9,
571 10.3390/atmos9010030, 2018.
572 Manca, G., Ammoscato, I., Esposito, G., Ianniello, A., Nardino, M., and Sprovieri, F.: Dynamics of snow-
573 air mercury exchange at Ny Ålesund during springtime 2011, E3S Web of Conferences, 1, 03010,
574 2013.
575 Maxwell, J. A., Holsen, T. M., and Mondal, S.: Gaseous elemental mercury (GEM) emissions from snow
576 surfaces in northern New York, Plos One, 8, e69342, 2013.
577 Motta, L. C., Blum, J. D., Johnson, M. W., Umhau, B. P., Popp, B. N., Washburn, S. J., Drazen, J. C.,
578 Benitez-Nelson, C. R., Hannides, C. C. S., Close, H. G., and Lamborg, C. H.: Mercury cycling in the
579 North Pacific subtropical gyre as revealed by mercury stable isotope ratios, Global Biogeochemical
580 Cycles, 33, 777-794, 10.1029/2018gb006057, 2019.
581 O'Connor, D., Hou, D., Ok, Y. S., Mulder, J., Duan, L., Wu, Q., Wang, S., Tack, F. M. G., and Rinklebe,
582 J.: Mercury speciation, transformation, and transportation in soils, atmospheric flux, and implications
583 for risk management: A critical review, Environment International, 126, 747-761,
584 10.1016/j.envint.2019.03.019, 2019.
585 Obrist, D., Faïn, X., and Berger, C.: Gaseous elemental mercury emissions and CO(2) respiration rates
586 in terrestrial soils under controlled aerobic and anaerobic laboratory conditions, Science of the Total
587 Environment, 408, 1691-1700, 2010.
588 Obrist, D.: Mercury distribution across 14 U.S. forests. Part II: Patterns of methyl mercury concentrations
589 and areal mass of total and methyl mercury, Environmental Science & Technology, 46, 7434, 2012.
590 Obrist, D., Pokharel, A. K., and Moore, C.: Vertical profile measurements of soil air suggest
591 immobilization of gaseous elemental mercury in mineral soil, Environmental Science & Technology,
592 48, 2242, 2014.
593 Obrist, D., Kirk, J. L., Zhang, L., Sunderland, E. M., Jiskra, M., and Selin, N. E.: A review of global

https://doi.org/10.5194/acp-2020-816
Preprint. Discussion started: 31 August 2020
© Author(s) 2020. CC BY 4.0 License.

environmental mercury processes in response to human and natural perturbations: Changes of emissions, climate, and land use, Ambio, 47, 116-140, 10.1007/s13280-017-1004-9, 2018.

Olson, C., Jiskra, M., Biester, H., Chow, J., and Obrist, D.: Mercury in Active-Layer Tundra Soils of Alaska: Concentrations, Pools, Origins, and Spatial Distribution, Global Biogeochemical Cycles, 32, 1058-1073, 10.1029/2017gb005840, 2018.

Osterwalder, S., Sommar, J., Akerblom, S., Jocher, G., Fritsche, J., Nilsson, M. B., Bishop, K., and Alewell, C.: Comparative study of elemental mercury flux measurement techniques over a Fennoscandian boreal peatland, Atmospheric Environment, 172, 16-25, 10.1016/j.atmosenv.2017.10.025, 2018.

Osterwalder, S., Huang, J.-H., Shetaya, W. H., Agnan, Y., Frossard, A., Frey, B., Alewell, C., Kretzschmar, R., Biester, H., and Obrist, D.: Mercury emission from industrially contaminated soils in relation to chemical, microbial, and meteorological factors, Environmental Pollution, 250, 944-952, 10.1016/j.envpol.2019.03.093, 2019.

Outridge, P. M., Mason, R. P., Wang, F., Guerrero, S., and Heimburger-Boavida, L. E.: Updated global and oceanic mercury budgets for the united nations global mercury assessment 2018, Environmental Science & Technology, 52, 11466-11477, 10.1021/acs.est.8b01246, 2018.

Pan, L., Lin, C.-J., Carmichael, G. R., Streets, D. G., Tang, Y., Woo, J.-H., Shetty, S. K., Chu, H.-W., Ho, T. C., Friedli, H. R., and Feng, X.: Study of atmospheric mercury budget in East Asia using STEM-Hg modeling system, Science of the Total Environment, 408, 3277-3291, 10.1016/j.scitotenv.2010.04.039, 2010.

Pannu, R., Siciliano, S. D., and O'Driscoll, N. J.: Quantifying the effects of soil temperature, moisture and sterilization on elemental mercury formation in boreal soils, Environmental Pollution, 193, 138, 2014.

Peleg, M., Tas, E., Matveev, V., Obrist, D., Moore, C. W., Gabay, M., and Luria, M.: Observational evidence for involvement of nitrate radicals in nighttime oxidation of mercury, Environmental Science & Technology, 49, 14008, 2015.

Perez-Rodriguez, M., Biester, H., Aboal, J. R., Toro, M., and Martinez Cortizas, A.: Thawing of snow and ice caused extraordinary high and fast mercury fluxes to lake sediments in Antarctica, Geochimica Et Cosmochimica Acta, 248, 109-122, 10.1016/j.gca.2019.01.009, 2019.

Risch, M. R., DeWild, J. F., Gay, D. A., Zhang, L., Boyer, E. W., and Krabbenhoft, D. P.: Atmospheric mercury deposition to forests in the eastern USA, Environmental Pollution, 228, 8-18, 10.1016/j.envpol.2017.05.004, 2017.

Slemr, F., Weigelt, A., Ebinghaus, R., Bieser, J., Brenninkmeijer, C. A. M., Rauthe-Schoech, A., Hermann, M., Martinsson, B. G., van Velthoven, P., Boenisch, H., Neumaier, M., Zahn, A., and Ziereis, H.: Mercury distribution in the upper troposphere and lowermost stratosphere according to measurements by the IAGOS-CARIBIC observatory: 2014-2016, Atmospheric Chemistry and Physics, 18, 12329-12343, 10.5194/acp-18-12329-2018, 2018.

Sørbotten, L. E.: Hill slope unsaturated flowpaths and soil moisture variability in a forested catchment in Southwest China, MD, Department of Plant and Environmental Sciences, University of Life Sciences, 2011.

Spolaor, A., Barbaro, E., Cappelletti, D., Turetta, C., Mazzola, M., Giardi, F., Bjorkman, M. P., Lucchetta, F., Dallo, F., Pfaffhuber, K. A., Angot, H., Dommergue, A., Maturilli, M., Saiz-Lopez, A., Barbante, C., and Cairns, W. R. L.: Diurnal cycle of iodine, bromine, and mercury concentrations in Svalbard surface snow, Atmospheric Chemistry and Physics, 19, 13325-13339, 10.5194/acp-19-13325-2019,

https://doi.org/10.5194/acp-2020-816
Preprint. Discussion started: 31 August 2020
© Author(s) 2020. CC BY 4.0 License.

2019.

Teixeira, D. C., Lacerda, L. D., and Silva-Filho, E. V.: Foliar mercury content from tropical trees and its correlation with physiological parameters in situ, Environmental Pollution, 242, 1050-1057, 10.1016/j.envpol.2018.07.120, 2018.

Wang, Q., Luo, Y., Du, B., Ye, Z., and Duan, L.: Influencing factors of mercury emission flux from forest soil at tieshanping,chongqing, Environmental Science, 35, 1922-1927, 2014.

Wang, S., Feng, X., Qiu, G., Fu, X., and Wei, Z.: Characteristics of mercury exchange flux between soil and air in the heavily air-polluted area, eastern Guizhou, China, Atmospheric Environment, 41, 5584-5594, 2007.

Wang, X., Bao, Z., Lin, C.-J., Yuan, W., and Feng, X.: Assessment of global mercury deposition through litterfall, Environmental Science & Technology, 50, 8548-8557, 10.1021/acs.est.5b06351, 2016.

Wang, X., Lin, C.-J., Feng, X., Yuan, W., Fu, X., Zhang, H., Wu, Q., and Wang, S.: Assessment of regional mercury deposition and emission outflow in mainland China, Journal of Geophysical Research-Atmospheres, 123, 9868-9890, 10.1029/2018jd028350, 2018.

Wang, Z., Zhang, X., Xiao, J., Zhijia, C., and Yu, P.: Mercury fluxes and pools in three subtropical forested catchments, southwest China, Environmental Pollution, 157, 801-808, 10.1016/j.envpol.2008.11.018, 2009.

Wang, Z. H., Zhang, G., Wang, Y., Zhao, Y. X., and Sun, X. J.: Research on mercury flux between snow and air under the condition of seasonal snow cover environment, Journal of Agro-Environment Science, 32, 601-606, 2013.

Wright, L. P., Zhang, L., and Marsik, F. J.: Overview of mercury dry deposition, litterfall, and throughfall studies, Atmospheric Chemistry and Physics, 16, 13399-13416, 10.5194/acp-16-13399-2016, 2016.

Xin, M., and Gustin, M. S.: Gaseous elemental mercury exchange with low mercury containing soils: Investigation of controlling factors, Applied Geochemistry, 22, 1451-1466, 2007.

Zarate-Valdez, J. L., Zasoski, R. J., and Lauchli, A.: Short-term effects of moisture content on soil solution pH and soil Eh, Soil Science, 171, 423-431, 10.1097/01.ss.0000222887.13383.08, 2006.

Zdanowicz, C., Karlsson, P., Beckholmen, I., Roach, P., Poulain, A., Yumvihoze, E., Martma, T., Ryjkov, A., and Dastoor, A.: Snowmelt, glacial and atmospheric sources of mercury to a subarctic mountain lake catchment, Yukon, Canada, Geochimica Et Cosmochimica Acta, 238, 374-393, 10.1016/j.gca.2018.06.003, 2018.

Zhang, G., Wang, N., Ai, J.-C., Zhang, L., Yang, J., and Liu, Z.-Q.: Characteristics of mercury exchange flux between soil and atmosphere under the snow retention and snow melting control, Huan jing ke xue= Huanjing kexue, 34, 468-475, 2013.

Zhang, H., Lindberg, S. E., Marsik, F. J., and Keeler, G. J.: Mercury air/surface exchange kinetics of background soils of the tahquamenon river watershed in the Michigan Upper Peninsula, Water Air & Soil Pollution, 126, 151-169, 2001.

Zhang, H., Lindberg, S. E., Barnett, M. O., Vette, A. F., and Gustin, M. S.: Dynamic flux chamber measurement of gaseous mercury emission fluxes over soils. Part 1: simulation of gaseous mercury emissions from soils using a two-resistance exchange interface model, Atmospheric Environment, 36, 835-846, 2002.

Zhang, L., Zhou, P., Cao, S., and Zhao, Y.: Atmospheric mercury deposition over the land surfaces and the associated uncertainties in observations and simulations: a critical review, Atmospheric Chemistry and Physics, 19, 15587-15608, 10.5194/acp-19-15587-2019, 2019.

Zhang, Q., Huang, J., Wang, F., Mark, L., Xu, J., Armstrong, D., Li, C., Zhang, Y., and Kang, S.: Mercury

https://doi.org/10.5194/acp-2020-816
Preprint. Discussion started: 31 August 2020
© Author(s) 2020. CC BY 4.0 License.

Atmospheric Chemistry and Physics Discussions

682 distribution and deposition in glacier snow over western China, Environmental science & technology,
683 46, 5404, 2012.
684 Zhou, J., Wang, Z., Zhang, X., and Chen, J.: Distribution and elevated soil pools of mercury in an acidic
685 subtropical forest of southwestern China, Environmental Pollution, 202, 187-195,
686 10.1016/j.envpol.2015.03.021, 2015.
687 Zhou, J., Wang, Z., Zhang, X., and Gao, Y.: Mercury concentrations and pools in four adjacent coniferous
688 and deciduous upland forests in Beijing, China, Journal of Geophysical Research: Biogeosciences,
689 122, 1260-1274, 2017a.
690 Zhou, J., Wang, Z., Zhang, X., and Sun, T.: Investigation of factors affecting mercury emission from
691 subtropical forest soil: A field controlled study in southwestern China, Journal of Geochemical
692 Exploration, 176, 128-135, 10.1016/j.gexplo.2015.10.007, 2017b.
693 Zhou, J., Wang, Z., and Zhang, X.: Deposition and fate of mercury in litterfall, litter, and soil in coniferous
694 and broad-leaved forests, Journal of Geophysical Research-Biogeosciences, 123, 2590-2603,
695 10.1029/2018jg004415, 2018.
696 Zhou, J., Du, B., Shang, L., Wang, Z., Cui, H., Fan, X., and Zhou, J.: Mercury fluxes, budgets, and pools
697 in forest ecosystems of China: A review, Critical Reviews in Environmental Science and Technology,
698 50, 1411-1450, 2020.
699 Zhu, W., Lin, C. J., Wang, X., Sommar, J., Fu, X., and Feng, X.: Global observations and modeling of
700 atmosphere-surface exchange of elemental mercury: a critical review, Atmospheric Chemistry &
701 Physics, 16, 4451-4480, 2016.
702

https://doi.org/10.5194/acp-2020-816
Preprint. Discussion started: 31 August 2020
© Author(s) 2020. CC BY 4.0 License.

703 **Table 1.** Locations and detailed measurements of soil-air TGM flux and environmental parameters at ten plots at the subtropical and temperate forests.

Forest	Plots	Locations	Flux (ng m^{-2} hr^{-1})	Soil surface TGM (ng m^{-3})	Soil Hg concentration (ng g^{-1})	SOM (0-5, %)	Soil moisture (%)	Soil temperature (℃)	Solar radiation (W m^{-2})
Subtropical forest	Plot S-A	Top-slope of coniferous forest	2.8 ± 3.9	3.6±1.3	219±15	13.6	0.3±0.1	16.8±7.6	39.9±27.5
	Plot S-B	Middle-slope of coniferous forest	3.5 ± 4.2	3.8±1.3	263±22	16.3	0.4±0.1	16.9±7.7	40.2±27.5
	Plot S-C	Wetland	-0.80 ± 5.1	3.7±1.4	96±43	4.9	0.3±0.1	16.7±7.5	30.5±27.9
	Plot S-D	Broad-leaved forest	0.18 ± 4.3	3.3±1.4	156±17	8.8	0.3±0.1	16.9±7.6	20.3±27.9
	Plot S-E	Open field	24 ± 33	4.1±1.7	159±18	4.1	0.3±0.1	18.3±8.5	98.0±138.4
Temperate forest	Plot T-A	Chinese pine forest	-0.04±0.81	2.22±0.87	72±12	5.8	17.0±8.55	9.77±6.57	17.09±29.4
	Plot T-B	Larch forest	0.32±0.96	2.30±0.94	141±15	25	26.3±6.51	10.0±6.23	22.9±18.6
	Plot T-C	Wetland	3.81±0.52	2.47±0.92	156±21	47	42.9±8.22	10.0±6.55	22.1±19.4
	Plot T-D	Mixed broad-leaved forest	0.68±1.01	2.37±0.87	74±9	16	25.4±7.32	9.86±6.26	25.9±18.6
	Plot T-E	Open field	1.82±0.79	1.98±0.79	52±4	12	27.9±5.56	10.1±6.47	47.1±29.4

704

Atmospheric Chemistry and Physics Discussions
Open Access
EGU

https://doi.org/10.5194/acp-2020-816
Preprint. Discussion started: 31 August 2020
© Author(s) 2020. CC BY 4.0 License.

Atmospheric Chemistry and Physics Discussions

Figure captions:

Fig. 1. Location of the five sampling plots and the estimation of Hg mass-balance at the temperate and subtropical forest. UR, SR, TF, LF and SA represents groundwater drainage, surface runoff, throughfall, litterfall and soil-air flux. Potential vegetation of China is from the Vegetation Map of China (Hou, 1982).

Fig. 2. Mean and standard deviation of soil-air TGM fluxes at the five plots for the four seasons and annual values during the study at the subtropical forest (A) and temperate forest (B). The number of flux observations in spring, summer, autumn and winter were 62, 92, 66 and 43 at the subtropical forest and 60, 58, 60 and 14 for the temperate forest, respectively.

Fig. 3. Daily (average flux of day and night) composite Hg flux, solar radiation and soil temperature at Masson pine forests (A) and (B), wetland (C), evergreen broad-leaved forest (D) and open field (E) at the subtropical forest. The vertical arrow represents rainy day.

Fig. 4. Daily (average flux of day and night) composite Hg flux, solar radiation and soil temperature at Chinese pine forest (A), larch forest (B), wetland (C), mixed broad-leaved forest (D) and open field (E) at the temperate forest. The vertical arrow represents rainy day.

Fig. 5. Correlation between the air TGM concentration and air-surface Hg flux measured in daytime and night for at Masson pine forests (A) and (B), wetland (C), evergreen broad-leaved forest (D) and open field (E) at the subtropical forest.

Fig. 6. Correlation between the air TGM concentration and air-surface Hg flux measured in daytime and night for the five plots at Chinese pine forest (A), larch forest (B), wetland (C), mixed broad-leaved forest (D) and open field (E) at the temperate forest.

Fig. 7. The diurnal patterns of soil Hg fluxes with meteorological parameters in spring (a), summer (b), autumn (c) and winter (d) at the coniferous forest of the subtropical forest.

Fig. 8. The diurnal patterns of soil Hg fluxes with meteorological parameters in spring (a), summer (b), autumn (c) and winter (d) at the deciduous broad-leaved forest of the temperate forest.

https://doi.org/10.5194/acp-2020-816
Preprint. Discussion started: 31 August 2020
© Author(s) 2020. CC BY 4.0 License.

Atmospheric Chemistry and Physics Discussions

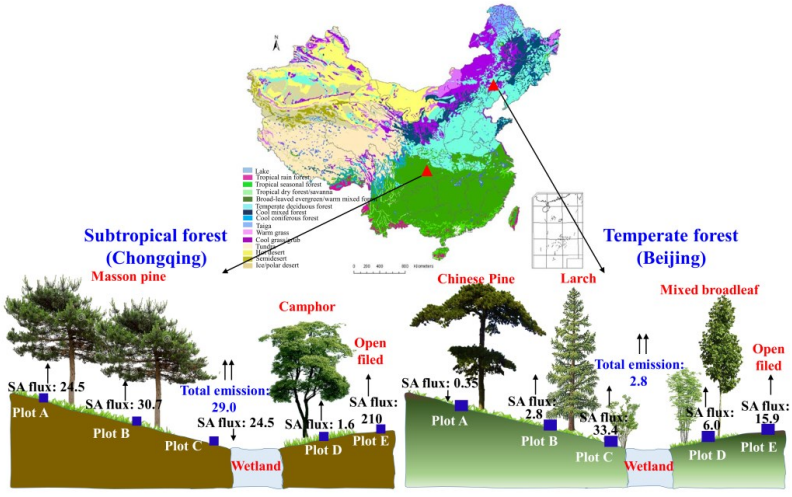

Fig. 1. Location of the five sampling plots and the estimation of Hg mass-balance at the temperate and subtropical forest. UR, SR, TF, LF and SA represents groundwater drainage, surface runoff, throughfall, litterfall and soil-air flux. Potential vegetation of China is from the Vegetation Map of China (Hou, 1982).

https://doi.org/10.5194/acp-2020-816
Preprint. Discussion started: 31 August 2020
© Author(s) 2020. CC BY 4.0 License.

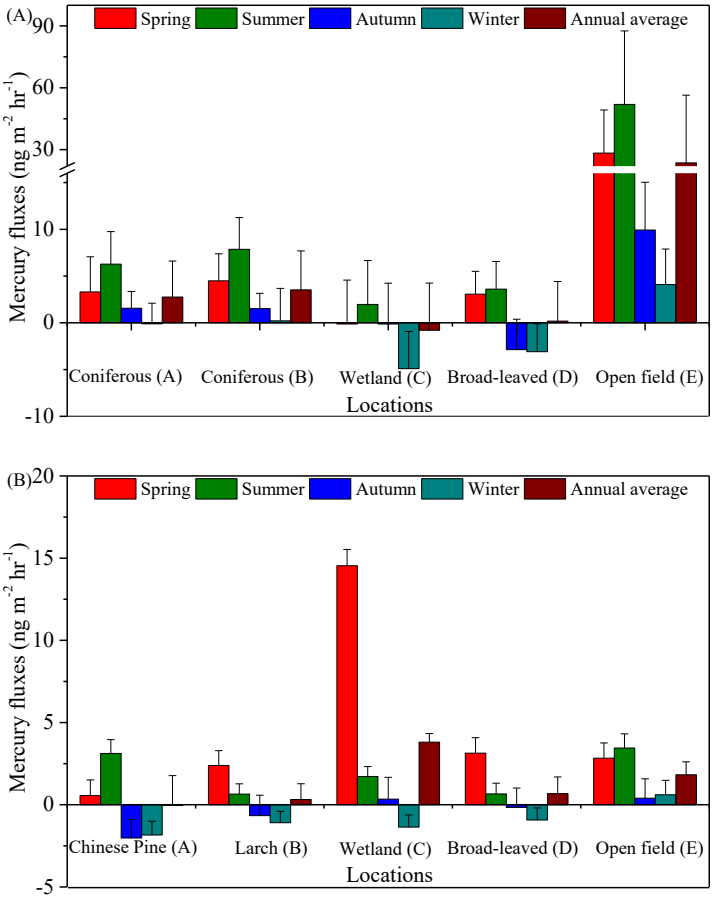

Fig. 2. Mean and standard deviation of soil-air TGM fluxes at the five plots for the four seasons and annual values during the study at the subtropical forest (A) and temperate forest (B). The number of flux observations in spring, summer, autumn and winter were 62, 92, 66 and 43 at the subtropical forest and 60, 58, 60 and 14 for the temperate forest, respectively.

https://doi.org/10.5194/acp-2020-816
Preprint. Discussion started: 31 August 2020
© Author(s) 2020. CC BY 4.0 License.

Atmospheric Chemistry and Physics Discussions

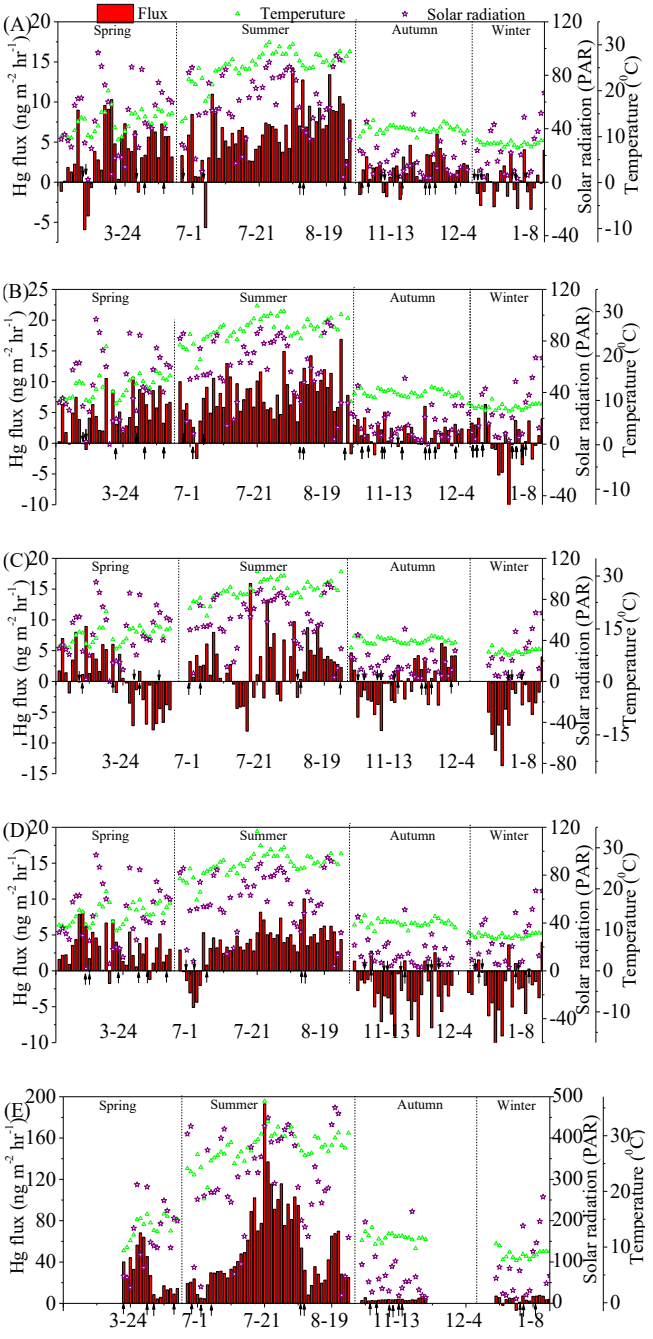

Fig. 3. Daily (average flux of day and night) composite Hg flux, solar radiation and soil temperature at Masson pine forests (A) and (B), wetland (C), evergreen broad-leaved forest (D) and open field (E) at the subtropical forest. The vertical arrow represents rainy day.

https://doi.org/10.5194/acp-2020-816
Preprint. Discussion started: 31 August 2020
© Author(s) 2020. CC BY 4.0 License.

Atmospheric Chemistry and Physics Discussions

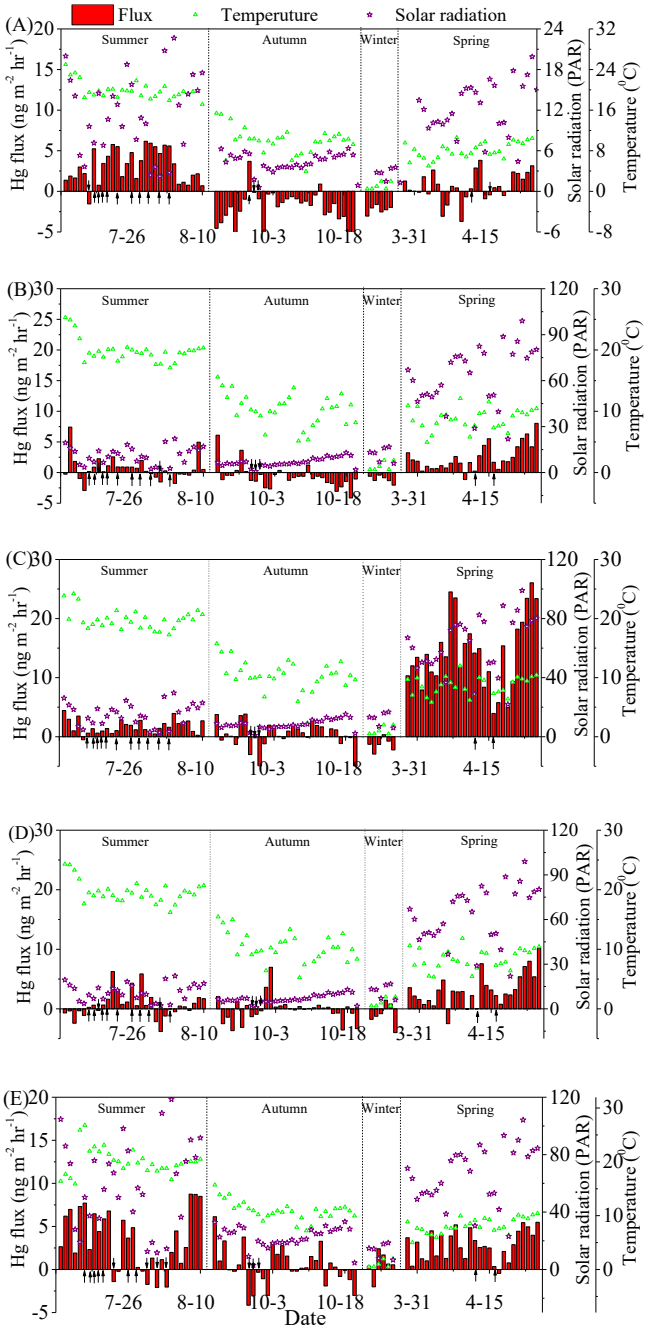

Fig. 4. Daily (average flux of day and night) composite Hg flux, solar radiation and soil temperature at Chinese pine forest (A), larch forest (B), wetland (C), mixed broad-leaved forest (D) and open field (E) at the temperate forest. The vertical arrow represents rainy day.

https://doi.org/10.5194/acp-2020-816
Preprint. Discussion started: 31 August 2020
© Author(s) 2020. CC BY 4.0 License.

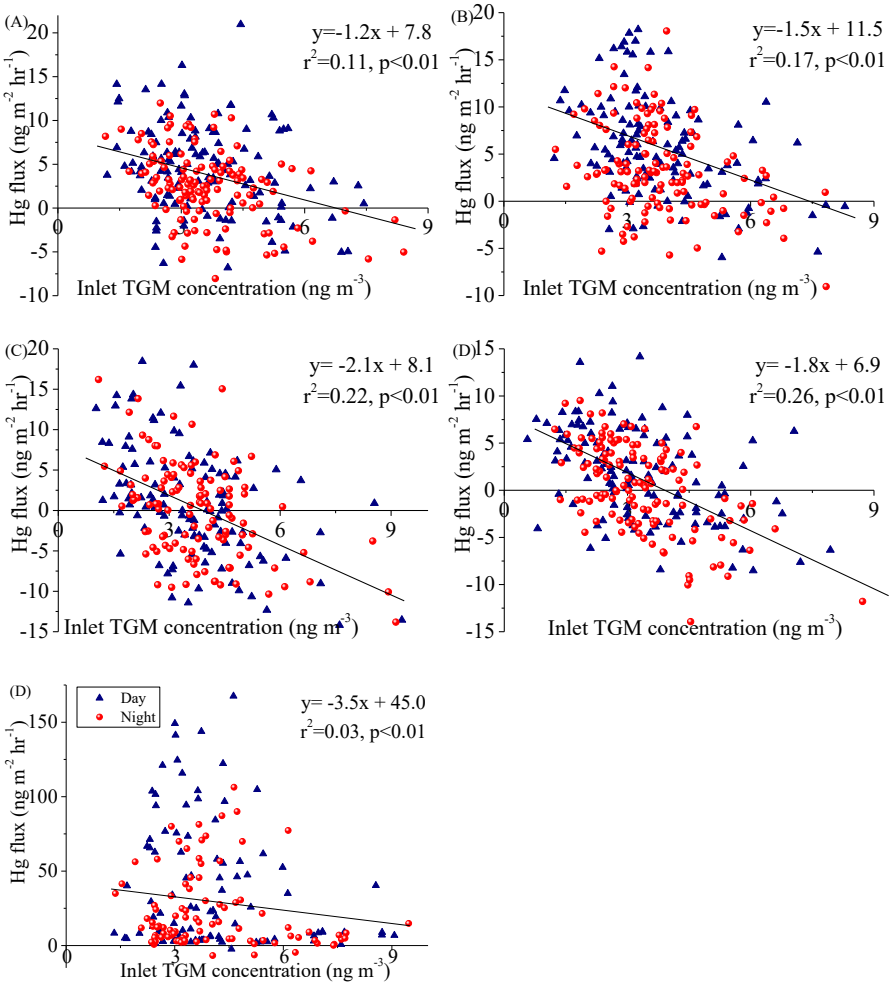

Fig. 5. Correlation between the air TGM concentration and air-surface Hg flux measured in daytime and night for at Masson pine forests (A) and (B), wetland (C), evergreen broad-leaved forest (D) and open field (E) at the subtropical forest.

https://doi.org/10.5194/acp-2020-816
Preprint. Discussion started: 31 August 2020
© Author(s) 2020. CC BY 4.0 License.

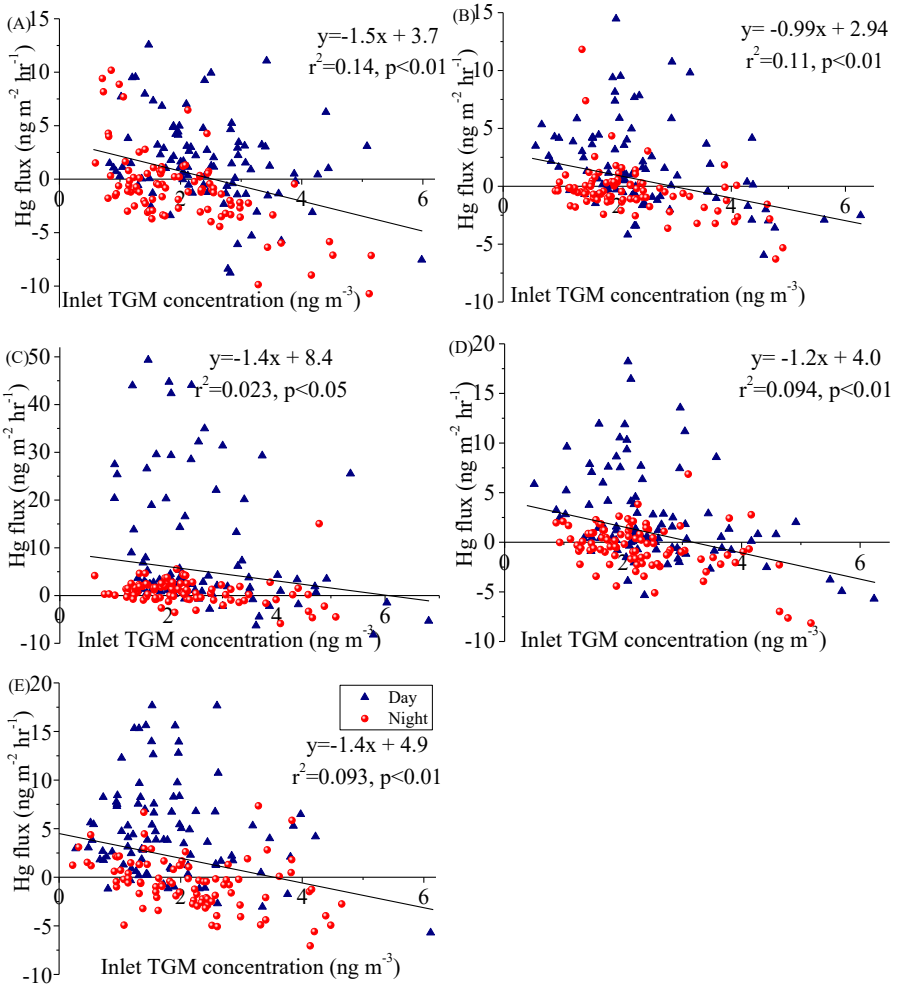

Fig. 6. Correlation between the air TGM concentration and air-surface Hg flux measured in daytime and night for the five plots at Chinese pine forest (A), larch forest (B), wetland (C), mixed broad-leaved forest (D) and open field (E) at the temperate forest.

https://doi.org/10.5194/acp-2020-816
Preprint. Discussion started: 31 August 2020
© Author(s) 2020. CC BY 4.0 License.

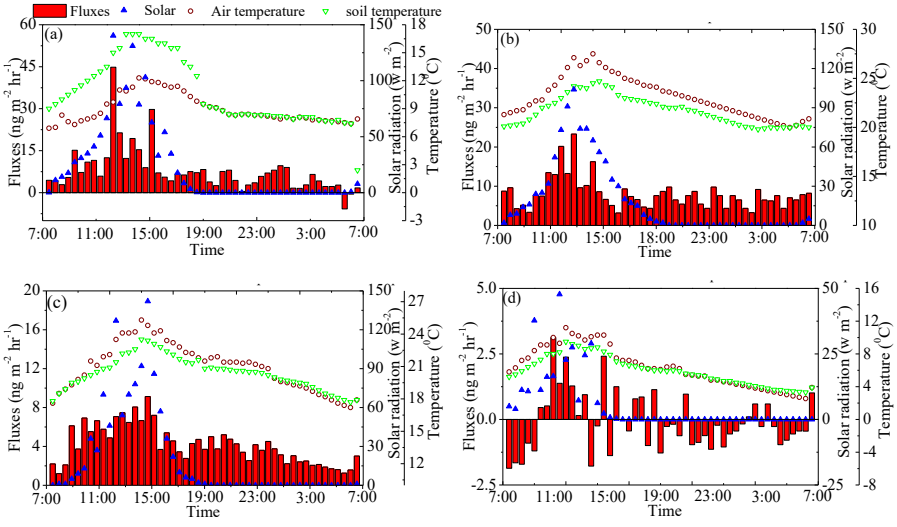

777

778

779 **Fig. 7.** The diurnal patterns of soil Hg fluxes with meteorological parameters in spring (a), summer
780 (b), autumn (c) and winter (d) at the coniferous forest of the subtropical forest.

781

782

https://doi.org/10.5194/acp-2020-816
Preprint. Discussion started: 31 August 2020
© Author(s) 2020. CC BY 4.0 License.

Atmospheric Chemistry and Physics Discussions

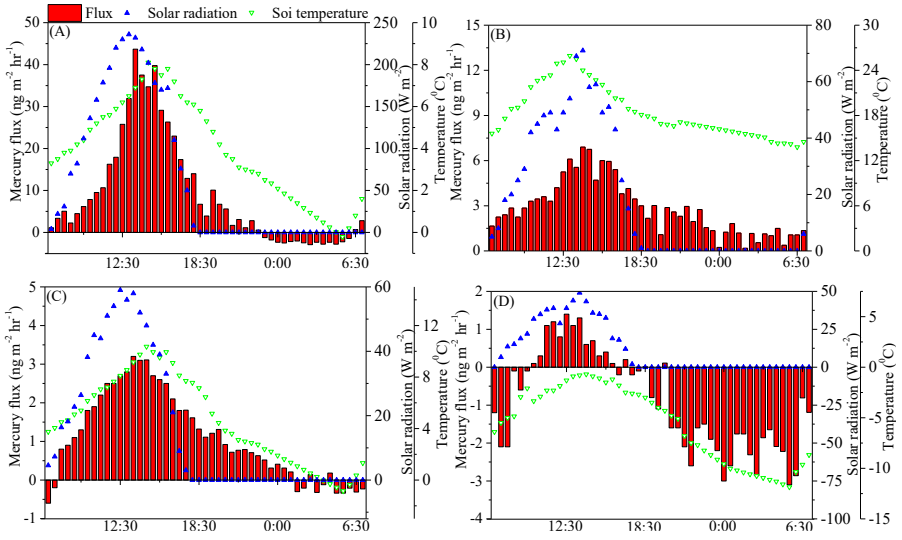

Fig. 8. The diurnal patterns of soil Hg fluxes with meteorological parameters in spring (a), summer (b), autumn (c) and winter (d) at the deciduous broad-leaved forest of the temperate forest.